

# Photometric redshifts in the Hubble Deep Fields: evolution of extinction and the star-formation rate.

Michael Rowan-Robinson

*Astrophysics Group, Blackett Laboratory, Imperial College of Science Technology and Medicine, Prince Consort Road, London SW7 2BW*

3 November 2018

## ABSTRACT

Photometric redshifts are studied with a template approach using data from HDF-N and -S. The problem of aliasing in photometric redshift estimates is investigated in some detail and found not to be a significant problem if at least four photometric bands are available. The performance of the approach presented here appears to exceed that of others in the literature. The rms accuracy of the photometric redshifts is 9.6 % in  $(1+z)$ , with a 1.5 % chance of a significant alias when four or more photometric bands are used.

With reasonable restrictions, it is possible to determine the dust extinction as well as the photometric redshift, provided five or more photometric bands are available. An important result is that evolution of  $\langle A_V(z) \rangle$  with redshift is seen, with higher values than locally at  $z = 0.5$ -1.5, and lower values at  $z > 2$ . This is consistent with current models for the star formation history of the universe.

Deconvolving the uv-to-ir seds into an old star and young star component allows determination of  $M_*$  and  $\dot{M}_*$  for each galaxy, as well as  $z_{phot}$  and  $A_V$ , provided that infrared photometric bands are available. The expected trend of  $b = M_*/\dot{M}_*t_0$  increasing to the past is seen. However there is a great deal of scatter in the relation between  $b$  and sed type, showing that the recent star-formation history is not very well correlated with the long-term history of a galaxy.

The 2800 Å luminosity function and star-formation rate are calculated for a large sample of HDF-N (2490) and HDF-S (28719) galaxies, using photometric redshifts, for the redshift range 0.2-5. The star-formation rates agree reasonably well with those from a variety of other uv,  $H_\alpha$ , infrared and submillimetre estimates, and with star-formation histories used to model optical, infrared and submillimetre source-counts.

**Key words:** infrared: galaxies - galaxies: evolution - star:formation - galaxies: starburst - cosmology: observations

## 1 INTRODUCTION

The Hubble Deep Field provided an important breakthrough in our understanding of the evolution of galaxies, permitting for the first time an analysis of the star-formation history of the universe out to redshift 4 (Madau et al 1996). Madau et al concluded that the star-formation rate was quite strongly peaked at redshift 1-2, and declined sharply at higher redshifts (see also Madau et al 1998). This decline at

high redshift was at least partly due to the neglect of extinction by dust, which several subsequent studies have shown to be an important effect (Rowan-Robinson et al 1997, Meurer et al 1997, 1999, Pettini et al 1998, Cram 1998, Steidel et al 1999, Adelberger and Steidel 2000, Hopkins et al 2001, Sullivan et al 2001). The correction for dust extinction remains highly uncertain, even for nearby galaxies, and few studies of the star formation history take any account of the expected evolution of the dust opacity in galax-

ies with epoch. Typical estimates of dust correction factors in the ultraviolet are 2-7. A new estimate of the average dust extinction in local galaxies has been made by Rowan-Robinson (2003) using ultraviolet, blue and far infrared data. When the contribution of the heavily extinguished starburst component is subtracted from the far infrared fluxes, the mean value of  $A_V$  in the interstellar mediums of nearby ( $V < 5000$  km/s) galaxies is found to be 0.31, corresponding to  $A_{2800} = 0.62$  for Milky Way dust.

In this paper I use large samples of galaxies in the Hubble Deep Fields (HDF), North and South, to study the evolution of the ultraviolet radiation-density, the dust opacity and hence the star formation history, using photometric redshift methods. I first study the issue of aliasing for photometric redshifts using fixed template photometric redshift estimates in HDF-N and HDF-S, comparing the results with those of other photometric redshift codes. I then investigate the effect of introducing extinction, characterized by  $A_V$ . Finally I also characterize the evolution of galaxy sed with redshift, using a new approach which separates the effects of young stars ( $< 10^9$  yrs old) and older stars. As might be expected the introduction of additional free parameters leads to increased aliasing, but also gives new insight into the evolution of dust extinction with redshift, and into the interpretation of the Hubble sequence.

The resulting photometric redshift catalogues are used to determine the uv luminosity function at a range of redshifts from 0.2 -5, the evolution of dust extinction and star-formation rate with redshift, and to estimate the stellar mass,  $M_*$ , and star formation rate,  $\dot{M}_*$ , in each galaxy.

A Hubble constant of 100 km/s/Mpc is used throughout.

## 2 PHOTOMETRIC REDSHIFTS IN THE HDF

The publication of the HST data on the HDF was an enormous stimulus to work on photometric redshift derivation. Lanzetta et al (1996), Mobasher et al (1996), and Gwyn and Hartwick (1996) used photometric redshift methods to assess the redshift distribution and properties of HDF galaxies. Madau et al (1996) used Lyman drop-out galaxies in the Hubble Deep Field to derive estimates for the star formation rate at  $z = 2 - 4.5$ . This analysis appeared to demonstrate that the star formation drops off steeply at  $z > 2$ . Connolly et al (1997) used photometric redshifts for the brighter HDF galaxies to derive the star formation rate at  $z = 0.5 - 2$ . Their method involved the use of J, H and K data in addition to the HST U,B,V,I data to determine the redshifts. Although this certainly improves the reliability of the photometric redshifts, it does restrict the analysis to galaxies with  $J < 23.5$ , ie a small fraction of the galaxies ( $< 10\%$ ) detected in

the HDF by HST. Fernando-Soto et al (1999) derived photometric redshifts for a larger sample of galaxies detected in 7 bands (UBVIJHK) and were able to test their predictions against the spectroscopic redshift catalogue of Cohen et al (2000). Pascarelle et al (1998) used the Lanzetta et al (1996) photometric redshifts to study the ultraviolet luminosity-density as a function of redshift. Lanzetta et al (2002) use their photometric redshifts to study the evolution of the surface brightness distribution function in galaxies. Arnouts et al (1999) have used photometric redshifts in HDF-N to study the redshift evolution of clustering and Teplitz et al (2001) have carried out a similar study with a much larger sample of galaxies in a 0.5 square degree field centred on HDF-S. Steidel et al (1999) have reanalyzed the HDF Lyman drop-out galaxies in HDF-N, to compare the results with their own Lyman drop-out surveys. Thompson et al (2001) used photometric redshifts to study the star-formation history using NICMOS data in HDF-N. Chen et al (2003) used photometric redshifts with the Las Campanas H-band survey to study the evolution of the rest-frame B-band luminosity function. A comparison of different photometric redshift methods was made by Hogg et al (1998).

All these studies used a set of fixed templates to determine photometric redshifts. Mobasher and Mazzei (1998) and Le Borgne and Rocca-Volmerange (2002) have used realistic, evolving galaxy sed to determine photometric redshifts.

Bolzonella et al (2000) have used simulations to study the effects of different choices of spectral energy distribution (sed) and photometric bands on the accuracy of photometric redshifts, and have included the effect of extinction as a free parameter.

### 2.1 Photometric redshifts using the template method

To try to extend the results of Connolly et al to a wider range of redshift, and to test the robustness of the conclusions of Madau et al (1996), I have used the photometric redshift method of Mobasher et al (1996) to analyze a much larger sample of HDF galaxies, namely all those galaxies with  $I_{AB} \leq 29.0$  from the catalogue of Williams et al (1996) detected in at least the I and V bands, a total of 2490 galaxies once duplicates have been eliminated. I have also analyzed in detail the problem of aliasing, which is central to the validity of the photometric redshift method.

As in Mobasher et al (1996) I use 6 galaxy spectral energy distributions, corresponding to E, Sab, Sbc, Scd, Sdm and starburst galaxies, based on the sed of Yoshii and Takahara (1988) and, for the starburst sed, Calzetti and Kinney (1992). The main changes from the work described in Mobasher et al (1996) are: (1) small modifications to sed, tuned to a preliminary list of 79 spectroscopic redshifts, (2) inclusion of J, H, K data summarized by Fernando-

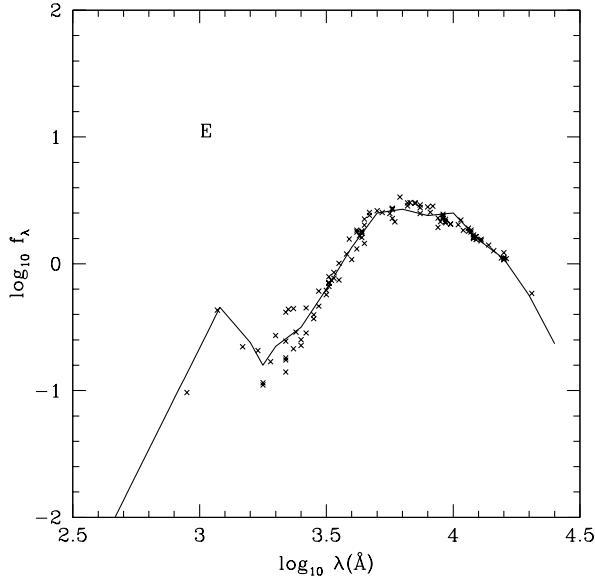


**Figure 1.** Assumed sed for elliptical galaxies (solid curve), with photometric data plotted for galaxies with spectroscopic redshifts (crosses).

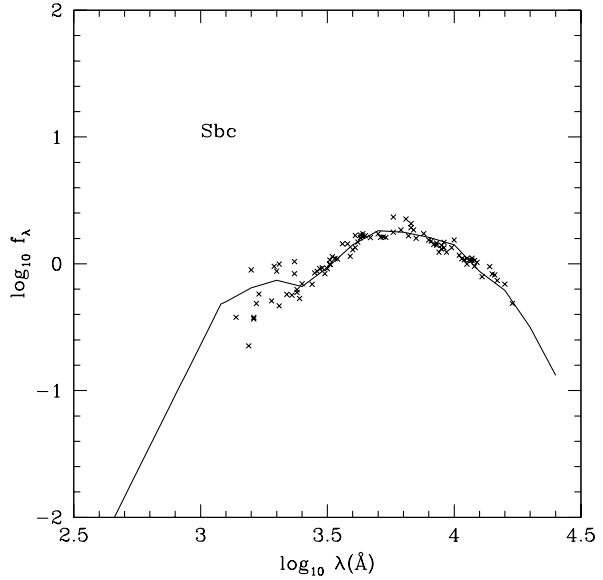


**Figure 3.** Assumed sed for Sbc galaxies, with data for galaxies with spectroscopic redshifts.

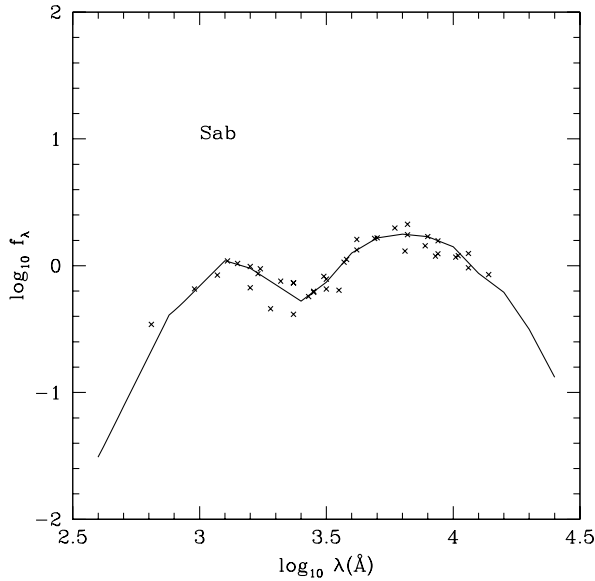


**Figure 2.** Assumed sed for Sab galaxies, with data for galaxies with spectroscopic redshifts.

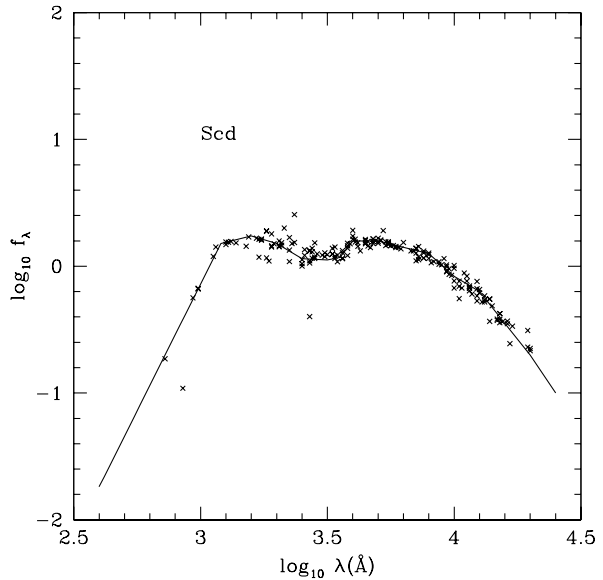


**Figure 4.** Assumed sed for Scd galaxies, with data for galaxies with spectroscopic redshifts.

Soto et al (1999), where available, (3) the solution is weighted with flux errors, where available (but to avoid excessively high weighting by very high signal-to-noise observations, the minimum flux error is assumed to be 5% of the flux), (4) the permitted maximum redshift is increased to 6, (5) the range of  $M(B)$  is restricted to the range -13.0 to -22.5 (to avoid excessive numbers of aliases at  $z = 0$  and 6), (6) dropouts

are treated as follows: if there is an upper limit in the U or B band which lies more than a factor 4 below the flux (in nJy) in the next shortest wavelength band, this upper limit is used in the photometric solution.

The sed's used are shown in Figs 1-6, compared with data for galaxies with known spectroscopic redshifts. Because different parts of these sed's are sampled by the HDF UBVI bands at different redshifts, different frequency ranges of these sed's have valid-

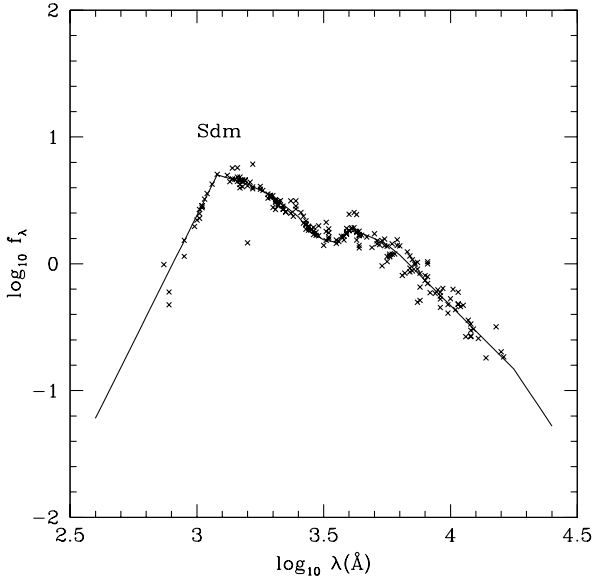


**Figure 5.** Assumed sed for Sdm galaxies, with data for galaxies with spectroscopic redshifts.

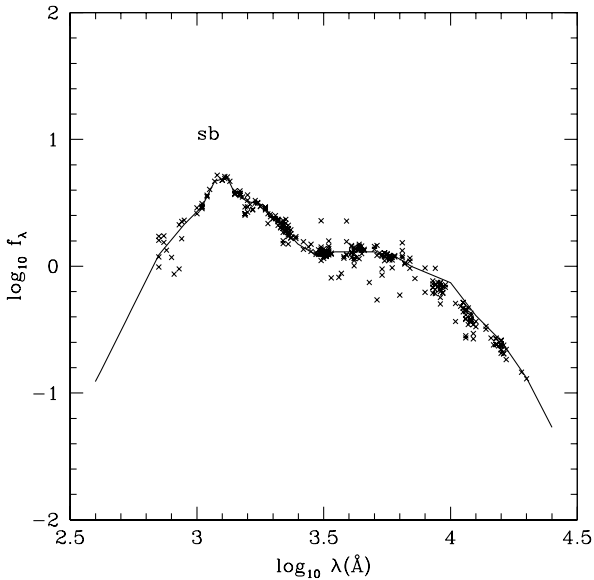


**Figure 6.** Assumed sed for starburst galaxies, with data for galaxies with spectroscopic redshifts.

ity over different redshift ranges. The number of sed used is quite critical to the success of the solution. Too few leads to what Bolzonella et al (2000) term 'catastrophic' failures, too many leads to increased aliasing and hence again to failures. Figs 1-6 illustrate that the 6 sed templates give a good low-resolution representation of the observed sed. Although a detailed treatment of the evolution of galaxy sed would improve the spectral resolution of the sed and would

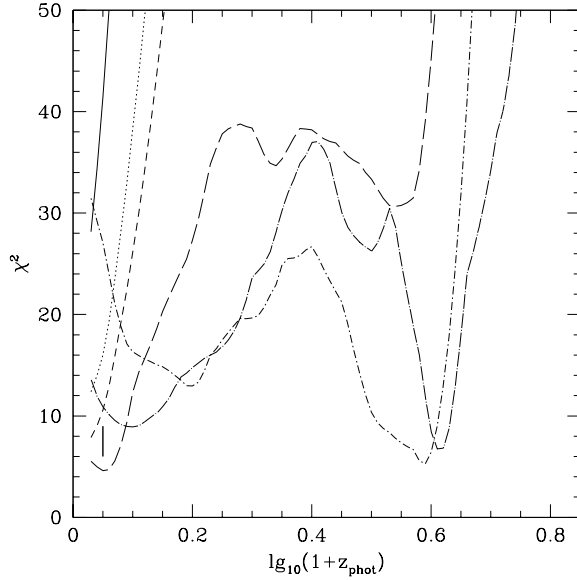


**Figure 7.** Reduced  $\chi^2$  ( $= \chi^2/(n - 2)$ ) as a function of  $lg_{10}(1 + z_{phot})$  for the 6 sed types, for HDF 4-916.0 ( $n=7$ ). The vertical bar denotes the minimum  $\chi^2$  at  $lg_{10}(1 + z_{phot}) = 0.05$ , and there are aliases at 0.10, 0.20, 0.59 and 0.61, of which the one at 0.59 is statistically significant. There is no minimum corresponding to the reported spectroscopic redshift at  $lg_{10}(1 + z_{spectr}) = 0.280$ .

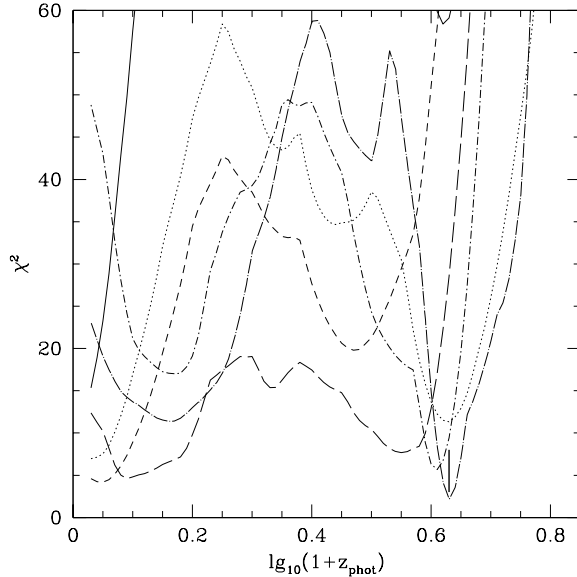


**Figure 8.** Reduced  $\chi^2$  as a function of  $lg_{10}(1 + z_{phot})$  for the 6 sed types, for HDF 4-52.111 ( $n=4$ ). The vertical bar denotes the minimum  $\chi^2$  at  $lg_{10}(1 + z_{phot}) = 0.63$ , and there are aliases at 0.05, 0.09, 0.55 and 0.61, none of which are statistically significant. The spectroscopic redshift is  $lg_{10}(1 + z_{spectr}) = 0.595$ . The FLY value is 0.107.

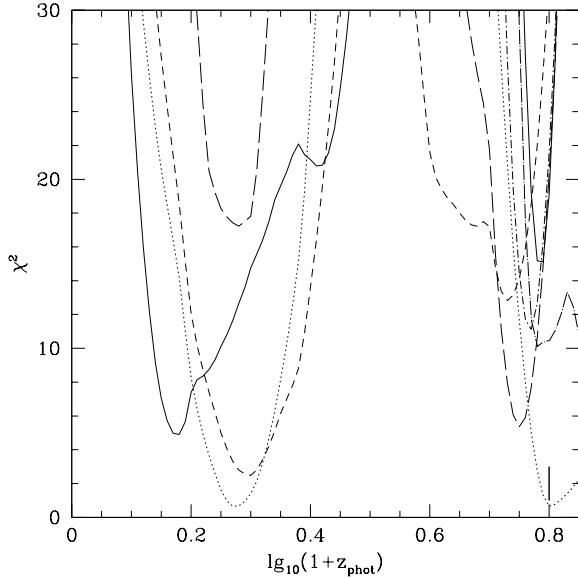


**Figure 9.** Reduced  $\chi^2$  as a function of  $lg_{10}(1+z_{phot})$  for the 6 sed types, for HDF 3-387.0 ( $n=4$ ). The vertical bar denotes the minimum  $\chi^2$  at  $lg_{10}(1+z_{phot}) = 0.80$ , and there is a significant alias at 0.27. The FLY value is 0.265.

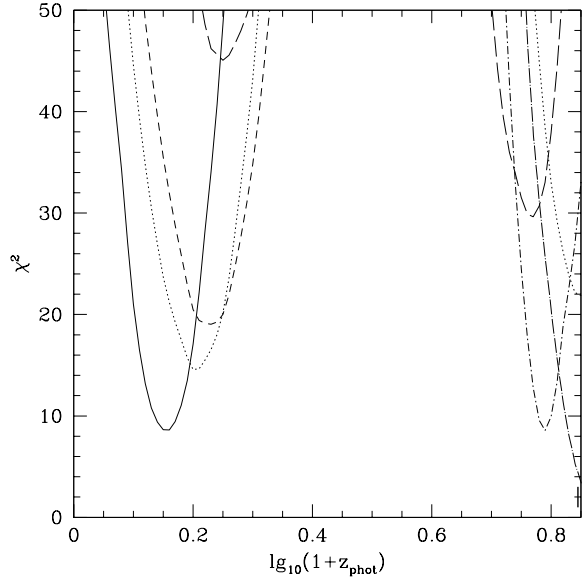


**Figure 10.** Reduced  $\chi^2$  as a function of  $lg_{10}(1+z_{phot})$  for the 6 sed types, for HDF 1-71.0 ( $n=6$ ). The vertical bar denotes the minimum  $\chi^2$  at  $lg_{10}(1+z_{phot}) = 0.85$ , and there are aliases at 0.16 and 0.76, but not statistically significant. The FLY value is 0.739.

probably improve the detailed fits, there is also likely to be an increased incidence of aliasing unless the observational data is also at improved spectral resolution. This seems to be borne out by the studies of Bolzanella et al (2000) and Le Borgne and Rocca-Volmerange (2003) (see section 2.3).

The percentage of galaxy sed types as a function of redshift, for  $z < 2.5$ , is shown in Table 1. The percentage of ellipticals drops at  $z > 1$ , as found by Rodighiero et al (2001) from imaging studies. The fraction of starburst galaxies increases steadily from 23% at  $z < 0.3$  to  $> 50\%$  at  $z > 1$ , consistent with the observed morphologies found by Lilley et al (1996). At higher redshifts the sed type is determined mainly by the sed of the most recent starburst and so has less connection with Hubble types.

One of the main problems in photometric redshift methods is aliasing. For a given set of photometric data, there may be two or more distinct redshifts, often, but not always, from different sed templates, which give an almost equally good representation of the data. Increasing the number of galaxy templates, and introducing other free parameters in the solution like extinction, may improve the accuracy of the redshift determination for the majority of galaxies, but at the expense of increasing the number of aliases, and hence of completely wrong redshifts. To try to make a quantitative estimate of the probability of aliasing, I proceed as follows. For each galaxy type and redshift bin, in the range 0.03 (0.01) 0.85 for  $lg_{10}(1+z_{phot})$ , I calculate  $\chi^2$ , and look for the minimum. I define a significant alias as a value of  $lg_{10}(1+z_{phot})$  differing

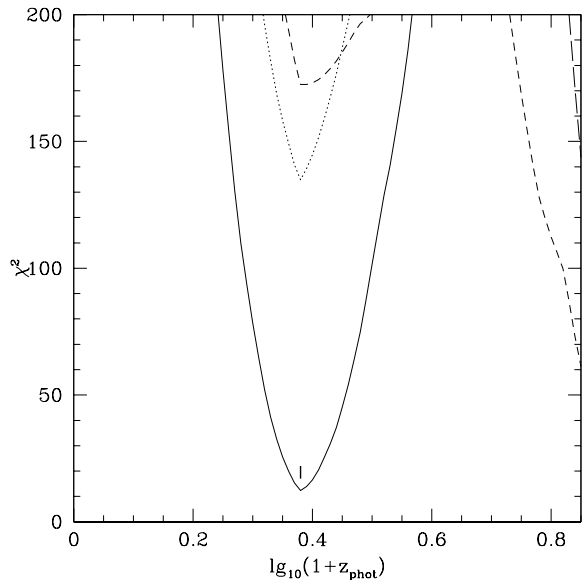


**Figure 11.** Reduced  $\chi^2$  as a function of  $lg_{10}(1+z_{phot})$  for the 6 sed types, for HDF 4-403.0 ( $n=6$ ), the galaxy in which a high redshift supernova has been observed (Riess et al 2001). The vertical bar denotes the minimum  $\chi^2$  at  $lg_{10}(1+z_{phot}) = 0.38$  ( $z = 1.4 \pm 0.05$ ). This is consistent with the estimate by Budivari et al (2000) of  $z = 1.55 \pm 0.15$  for this galaxy, but only marginally with the estimate  $1.7 \pm 0.1$  given for the supernova by Riess et al (2001).

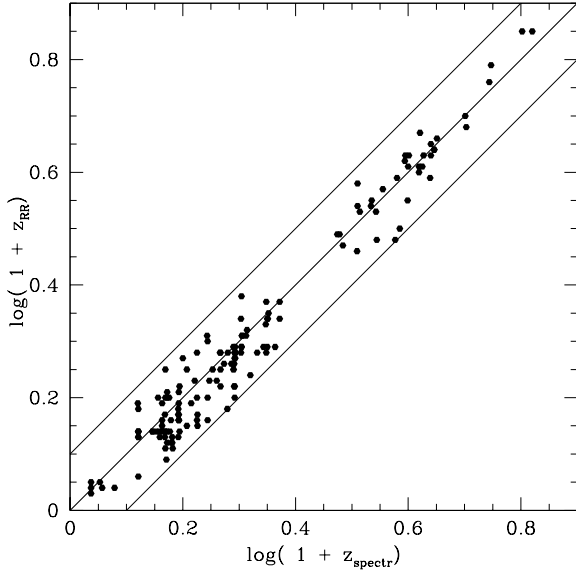


**Figure 12.** Photometric versus spectroscopic redshifts for 152 galaxies in the Hubble Deep Field (N), from template method of present paper. The rms value of  $\log_{10}[(1 + z_{ph})/(1 + z_{sp})]$  is 0.0398, corresponding to a 9.6% accuracy in photometric estimates of  $(1+z)$ .

from the minimum value by more than 0.08, ie  $(1+z)$  differs by more than 20%, with  $\chi^2$  no more than 1.0 above the minimum value (see figs 7-11 for examples). The proportions of galaxies with significant aliases then depends very strongly on the number of photometric bands in the solution,  $n$ , where presence of a significant dropout is included as a detected band. For  $n = 2, 3, 4, 5, 6, 7$ , the proportions are 99, 38, 1.5, 0.5, 0.0, 1.5%. Thus a minimum of 4 bands is needed for effective estimation of photometric redshifts. Very little weight can be attached to estimates based on 2 bands, of which there are 374 in our sample of 2470.

The comparison of photometric and spectroscopic redshifts for 152 HDF galaxies with spectroscopic redshifts in the literature is shown in Fig 12. The sample consists of 145 redshifts given in the data set of 1067 HDF galaxies given by Fernandez-Soto et al (1999, hereafter FLY), with the deletion of 4-555.2 and 3-550.1 (no longer listed as spectroscopic redshifts in Fernandez-Soto et al 2001 or Cohen et al 2000), the addition of 4-618.0 (Cohen 2001), and the corrected redshifts for 4-852.12, 2-906.0 and 2-256.0 given by Cohen (2001). In addition spectroscopic redshifts for 5 galaxies, for which all photometric redshift methods agree on a different redshift and find no alias at the quoted spectroscopic redshift, are deleted: 4-948.11111, 4-878.11, 3-355.0, 4-316.0, and 4-916.0. For the remaining 1423 galaxies in the Williams et al (1966) catalogue satisfying the constraints given at the beginning of section 2.1, there are a further 7 spectroscopic redshifts available.

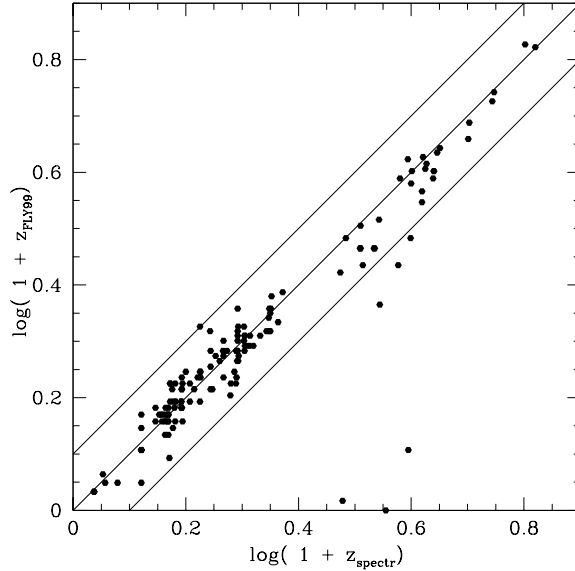


**Figure 13.** Photometric versus spectroscopic redshifts for 145 galaxies in the HDF-N, from Fernandez-Soto et al (1999).

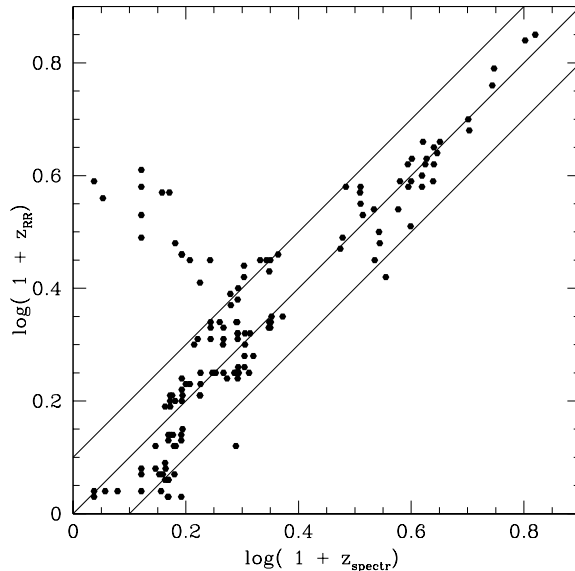


**Figure 14.** As for Fig 12, but using only 4 bands (UBVI).

My template method gives redshifts accurate to 9.6% in  $(1+z)$ . Bolzonella et al (2000) report an increase in the uncertainty in  $z_{phot}$  with redshift from their simulations but this does not seem to be the case for the more meaningful quantity  $(z_{phot} - z_{spect})(1 + z_{spect})$ .

Some individual discrepancies between photometric and spectroscopic redshifts are summarized in Table 2. For 7 objects my estimate agrees with the

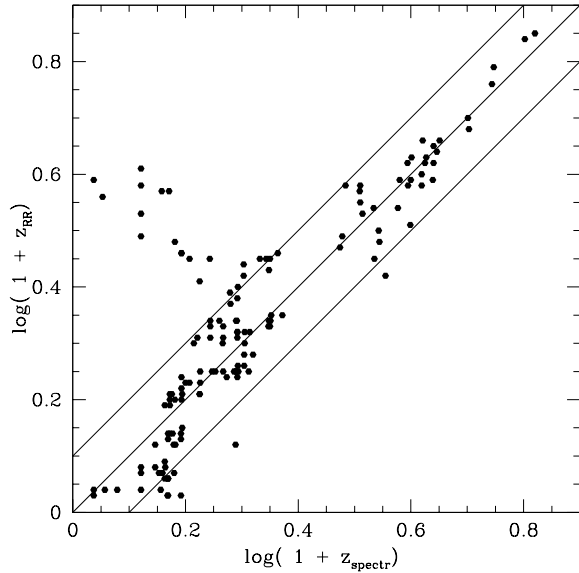


**Figure 15.** As for Fig 12, but using only 3 bands (UBV).

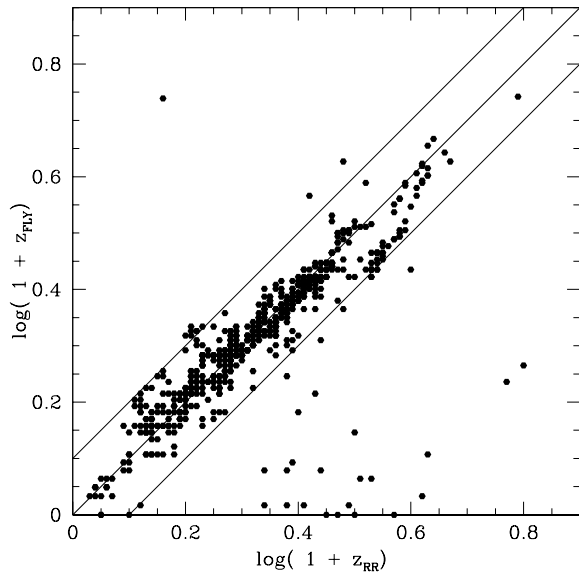


**Figure 16.** Comparison of photometric redshifts from present paper with those of FLY, for sources detected in at least 4 bands.

spectroscopic redshift within 0.1 in  $\log_{10}(1+z)$ , but the Fernando-Soto et al (1999) estimate disagrees: 4 of these have been fixed by the revisions applied in Fernando-Soto et al (2001). On this basis my photometric redshift estimates appear marginally better than those of Fernando-Soto et al. The concordant redshifts in Fig 12 include 7 cases where only 3 bands were detected and 2 where only 2 bands were detected, so even though these galaxies have significant

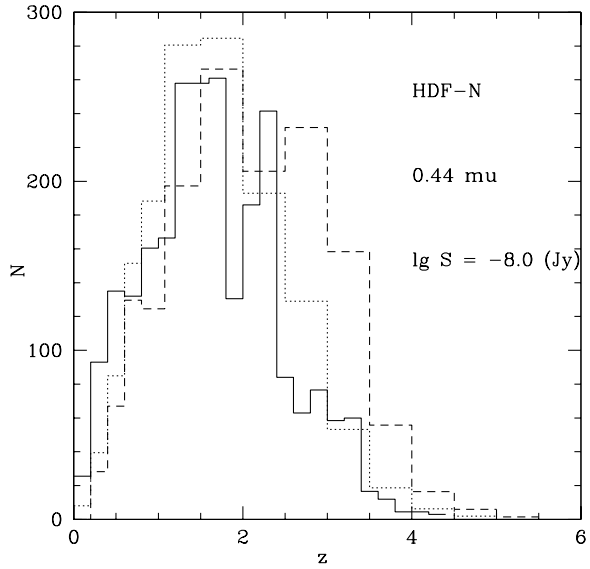


**Figure 17.** Redshift distribution for the Hubble Deep Field (N). The solid histogram is derived from photometric redshifts, as described in section 3, for  $B < 29$ . The broken histogram is the prediction from the  $\lambda_o = 0.7$  model of Rowan-Robinson (2001), for  $S(0.44 \mu\text{m}) = 10 \text{ nJy}$  and the dotted curve is the corresponding model of King and Rowan-Robinson (2003).

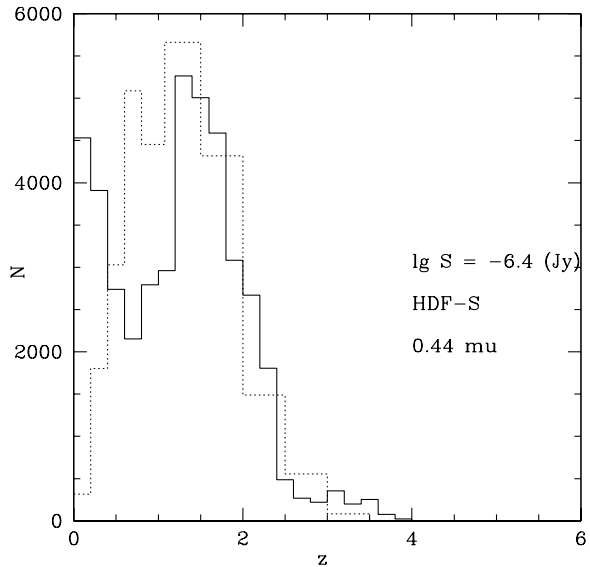


**Figure 18.** Redshift distribution for the Hubble Deep Field (S). The solid histogram is derived from photometric redshifts, as described in section 3, for  $B < 25$ . The broken histogram is the prediction from the  $\lambda_o = 0.7$  model of Rowan-Robinson (2001), for  $S(0.44 \mu\text{m}) = 400 \text{ nJy}$ .

aliases the method has selected the correct redshift. Figure 13 shows the corresponding comparison for Fernandez-Soto et al (1999). Figure 14 shows what happens to my photometric redshift estimates if I use only the 4 bands U, B, V, I. For only one galaxy does the photometric redshift become strongly discrepant, confirming that for a high proportion of cases 4-band estimates are reliable. On the other hand if only 3 bands (U, B, V) are used (Fig 15), about 20% of the photometric estimates are discrepant. This is entirely consistent with the success that Steidel et al (1998) have had using the Lyman dropout technique with 3 photometric bands, with 75 % of their U-band dropout galaxies have spectroscopic redshifts in the range 2.7-3.3.

Fig 16 shows a direct comparison of photometric redshift estimates by Fernandez-Soto et al (1999) and myself, for galaxies detected in at least four photometric bands. The agreement is extremely good, with only 38/688 estimates being discrepant. The group of galaxies for which Fernandez-Soto et al give significantly lower redshift estimates include three galaxies in Table 1 for which the spectroscopic redshift appears to confirm my estimate. The greater scatter appearing in the comparison of photometric redshift estimates by Fernandez-Soto et al and myself made by Peacock et al (2000, their Fig 1) arises because this comparison includes estimates based on only 2 or 3 photometric bands. Table 3 lists the 33 galaxies which I estimate to have  $z > 5$ , together with spectroscopic measurements (3 cases) and estimates by Fernandez-Soto et al (1999). For 4 of the galaxies Fernandez-Soto et al estimate low redshifts: these are all cases where I find a significant alias (an example is shown in Fig 9). Otherwise the agreement is reasonable, but with a tendency for my redshifts to be slightly higher than those of Fernandez-Soto et al (and than the spectroscopic redshifts, where available).

Fontana et al (2000) find a rather poor performance of their photometric redshift estimates when only four photometric bands are used (their Fig 10), in contrast to the excellent results obtained here. Similarly the Bolzonella et al (2000) 'hyperz' code has quite a significant proportion of failures with 4 or even 5 bands (their Fig 2). I also have no problems with the 2 galaxies 4-473.0 and 4-52.111 (see fig 8, present paper), for which Bolzonella et al (2000) report catastrophic failure with 6 different sed prescriptions (their Fig 4). I conclude that my code is more robust than those of Fontana et al (2000) and Bolzonella et al (2000).

My photometric redshift estimate for HDF 4-403.0, in which Riess et al (2001) have detected a supernova, is  $1.4 \pm 0.05$  (see fig 11), consistent with the estimate by Budavari et al (2000) of  $1.55 \pm 0.15$  but only marginally consistent with the estimate of  $1.7 \pm 0.1$  derived by Riess et al (2001) for the supernova.

The redshift distribution derived above for HDF-

N galaxies with  $B < 29$  is shown in Fig 17, compared with the predictions of the models of Rowan-Robinson (2001) and King and Rowan-Robinson (2003) for an  $\lambda_o = 0.7$  universe. The King and Rowan-Robinson (2003) model fits well, while the Rowan-Robinson (2001) model predicts too many galaxies at  $z > 2.5$ .

The Goddard Space Flight Center Group (Teplitz et al 2001) have published UBVRI data for galaxies in a 0.5 square degree area centred on HDF-S. After elimination of objects characterized as stars, there are 28719 galaxies in their  $5-\sigma$  catalogue and I have used these to estimate photometric redshifts as above. I have compared my estimates with the spectroscopic redshifts of Glazebrook et al (2001), and like Teplitz et al (2001) I find good agreement if the comparison is restricted to Glazebrook et al's quality 3 and 4 redshifts. Figure 18 shows the photometric redshift distribution for galaxies from this catalogue with  $B < 25$ , which appears to be the completeness limit, compared with predictions of the model by Rowan-Robinson (2001). The agreement is good except at low redshifts, where the star-formation history derived for these data differs significantly from that assumed in the model (see Fig 28): this merits further investigation.

The combined 2800 Å luminosity function for HDF-N and HDF-S is then estimated for each redshift bin and fitted with a Schechter function. No correction for the effects of dust extinction has been applied at this stage. The results are summarized in Fig 19 for an  $\Omega_o = 1$  universe. The uncertainties given combine in quadrature the purely statistical uncertainties and the additional contribution to the scatter due to the use of photometric redshifts, which has been estimated from a series of simulations following the method of SubbaRao et al (1996). The distribution of  $\log_{10}(1+z)$  was assumed to be gaussian, with  $\sigma = 0.04$  where 4 or more bands are available, 0.06 if only 3 bands are available, and 0.08 if only 2 bands are available, to take account of the increased uncertainty where less than 4 bands are available. There are some discrepancies between estimates from HDF-N and HDF-S at luminosities where they overlap, but overall the agreement of the two datasets with each other, and with the models, is good.

I find that the best faint end slope of the luminosity function for the redshift range 0-4 is  $\alpha = 1.6$ , which is also the value found by Steidel et al (1999) for galaxies with  $z = 3$ . Figure 19 shows results assuming  $\alpha = 1.6$ . Most local studies at optical wavelengths find faint end slopes in the range  $\alpha = 1.1-1.3$ .

Lanzetta et al (2002) have used the HDF-N sample to study the surface brightness distribution function. They note that uncertainty in the shape of the faint end of this distribution at higher redshifts translates into a major uncertainty in the star-formation rate. In the present work, the larger HDF-N sample and the use of both HDF-N and -S samples provides sufficient dynamic range in luminosity, even at high

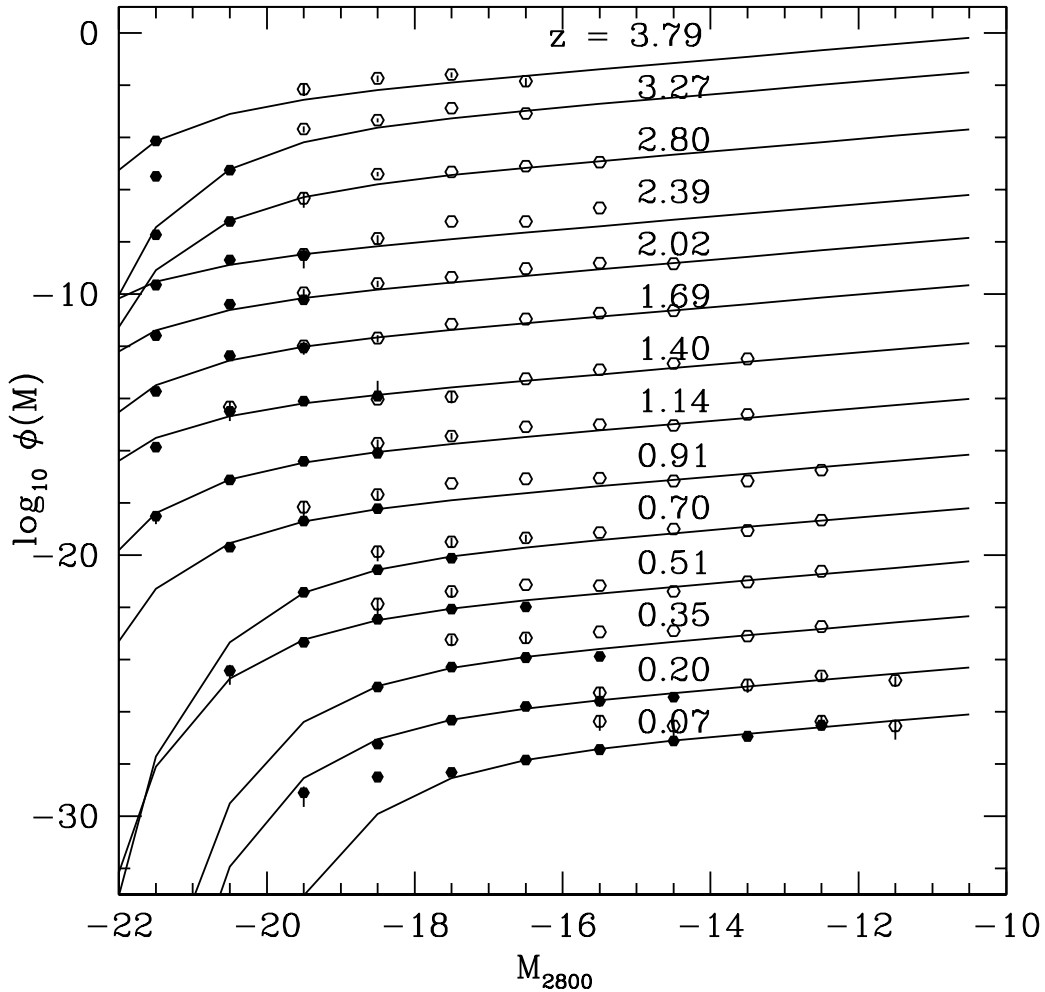


**Figure 19.** 2800 Å luminosity functions derived from HDF-N (open circles) and HDF-S (filled circles) photometric redshifts, in bins of 0.05 in  $\log_{10}(1+z)$ . No correction for dust extinction has been applied at this stage. The solid curves are best-fitting Schechter functions, with a faint-end slope  $\alpha = 1.6$ . An  $\Omega = 1$  universe is assumed.

redshift, that the uncertainty in the shape of the luminosity function and in the star-formation rate is less severe.

My values for  $M_{*,2800}$  at  $z = 0.70, 1.14, 1.40, 1.69$  (-18.5, -20.0, -20.6, -20.4) are reasonably consistent with those found by Connolly et al (1997) for  $z = 0.5-1, 1-1.5, 1.5-2$  (-18.75, -19.5, -20.25). In section 3, I will use these luminosity functions to estimate the evolution of the star-formation rate in galaxies, but first we need to consider the evolution of extinction in galaxies.

## 2.2 Effect of inclusion of $A_V$ as a free parameter

The semi-empirical sed templates used above can be assumed to already take account of an average

amount of internal extinction at  $z = 0$ . However we need to allow for the possibility of evolution of the average extinction with redshift, an effect predicted by Pei et al (1999) and Calzetti and Heckman (1999) for a variety of star formation histories. It is also clear from far infrared and submillimetre surveys that some galaxies have significantly higher extinctions than the average for their Hubble type (see also the study of local galaxies by Rowan-Robinson 2003).

Le Borgne and Rocca-Volmerange (2002) include in their models allowance for the evolution of the characteristic dust extinction with time. However to fully allow for the variation in dust extinction from galaxy to galaxy we really need to solve for  $A_V$  as a free parameter, in addition to the redshift. Since we are trying to do this with rather limited photometric data, this will inevitably result in increased aliasing. Basi-

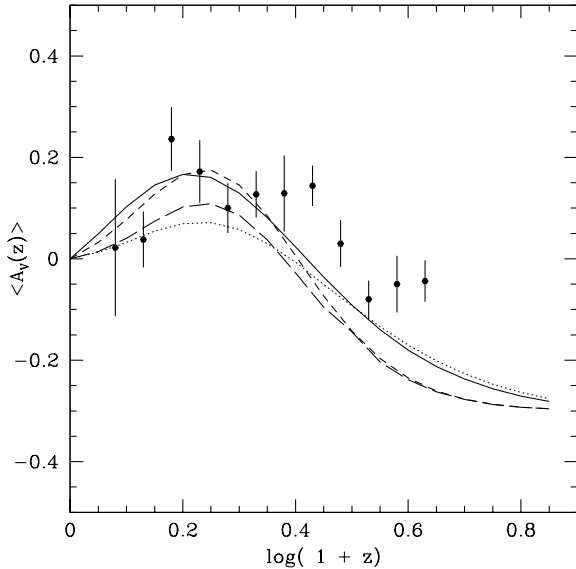


**Figure 20.** Variation of mean value of  $A_V$  with redshift, derived from HDFN. Curves are theoretical models calculated as described in Appendix, assuming that  $A_V(0) = 0.3$  (Rowan-Robinson 2003). Solid curve:  $\Omega_0 = 1$  (dotted curve: with density evolution as in King and Rowan-Robinson 2003); broken curves:  $\lambda_0 = 0.7$ .

cally an earlier Hubble type may look similar, over a restricted wavelength range, to a later type with substantial reddening. This aliasing problem seems to be born out by the study of Bolzanella et al (2001), who include  $A_V$  as a free parameter and have significantly worse aliasing problems than the pure template solution of section 2.1 above.

To try to control this aliasing problem to some extent, I have made the following restrictions: (i) I assume that there is no extinction in ellipticals. (ii)  $A_V$  is allowed to vary between -0.4 and + 1.0. Negative values are needed because we may expect  $A_V$  to be lower at high redshift than at the present epoch. The assumption is that the typical value of  $A_V$  at the present epoch in spirals is 0.3-0.4 mag (Rowan-Robinson 2003). The  $A_V$  we are solving for is the difference between the actual value and the mean value at the present epoch. (iii) No solution for  $A_V$  is sought if the reduced  $\chi^2$  for the solution with  $A_V = 0$  is  $< 0.01$  or if there are less than 3 bands available. (iv) A non-zero  $A_V$  is accepted only if the reduced  $\chi^2$ , allowing for the reduced number of degrees of freedom, is improved by the inclusion of  $A_V$ . (v) A prior expectation that the probability of a given value of  $A_V$  declines as  $|A_V|$  moves away from zero is introduced by minimizing  $\chi^2 + \alpha A_V^2$  rather than  $\chi^2$ .

Fig 20 shows the variation of  $\langle A_V(z) \rangle$  with redshift, calculated from different galaxy samples, compared with the prediction of closed box star formation models of the form used by Rowan-Robinson

(2001) and King and Rowan-Robinson (2003) (see Appendix). There is some evidence for the expected increase in  $\langle A_V(z) \rangle$  towards  $z = 1$ , and of the expected decrease at higher redshift. Fig 21 shows the distribution of  $\chi^2$ , with and without the inclusion of  $A_V$ . The inclusion of  $A_V$  does reduce many of the higher values of  $\chi^2$ .

The inference that the extinction in  $z \sim 3$  galaxies is smaller than in galaxies locally is at odds with the claim of Steidel et al (1999), supported by Adelberger and Steidel (2000) and Vijh et al (2003), that the extinction at  $z \sim 3$  is substantial,  $E(B-V) = 0.15$ . However it is noteworthy that these latter claims are based on a single colour, (G-R). In the case of the HDF-N sample we can do better than this, because most of the  $z \sim 3$  galaxies are detected at 4500, 6000 and 8000 Å. Fig 22 shows the [6000-8000] v. [4500-6000] colour-colour diagram for HDF-N galaxies with  $z = 3 \pm 0.4$ . The locations of my six galaxy templates corresponding to  $z = 3$  are indicated, as also is a reddening line from the starburst locus (sb). While some of the spread can be attributed to reddening, with  $E(B-V) \leq 0.1$ , the main elongation of the distribution is consistent with being due to different recent star-formation histories. Note the the location of the elliptical component (E) is due to the effect of planetary nebulae, not recent star-formation. Vijh et al (2003) claim that different star-formation histories can not account for the broad spread in (G-R) colours seen in the Lyman drop-out galaxies, but the models they consider allow only for different times since the start of star-formation. If we look instead at models for an instantaneous burst viewed at different times from the end of the burst (Bruzual and Charlot 1993, Fig 4a, or Bruzual 2000, Fig 1a), it is easy to see that the (G-R) colour from a  $z = 3$  galaxy changes by at least 2 magnitudes in 0.3 Gyr. However the age-dust degeneracy can be broken if infrared observations are available and Shapley et al (2001) do find consistency with the Steidel et al (1999)  $E(B-V)$  estimates from a sub-sample of 63  $z \sim 3$  galaxies with J and K measurements. Erb et al (2003) find better agreement between star-formation rates derived from uv continuum and  $H\alpha$  for 16 galaxies at  $2.0 < z < 2.6$  if a mean extinction of  $E(B-V) = 0.10$  is corrected for.

My photometric redshift catalogues for HDF-N, HFF and HDF-S, with parameters estimated by the template method both with  $A_V$  set = 0, and with  $A_V$  as a free parameter, are available at

<http://astro.ic.ac.uk/~mrr/photz> .

### 2.3 Inclusion of treatment of sed evolution

Mobasher and Mazzei (1998) and Le Borgne and Rocca-Volmerange (2002) have used spectral synthesis models to track the evolution of sed with redshift. In principle this should yield improved photometric redshifts compared with a fixed template method, since the latter can only be accurate over a fixed

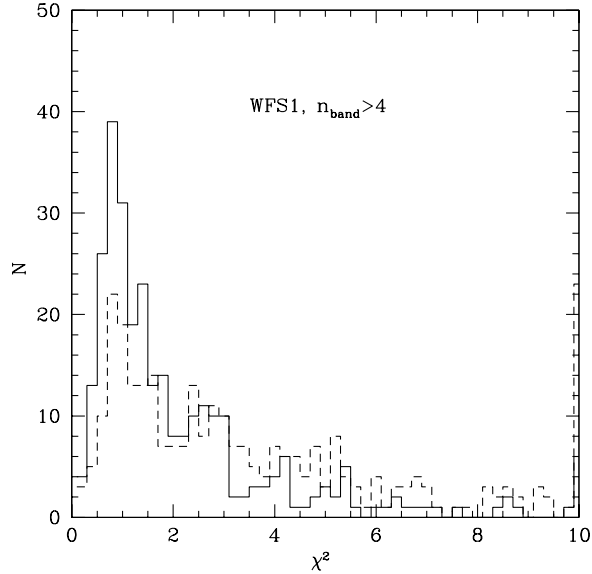


**Figure 21.** Plot of distribution of  $\chi^2$  with no correction for  $A_V$  (broken line), and including effect of  $A_V$  (solid line).

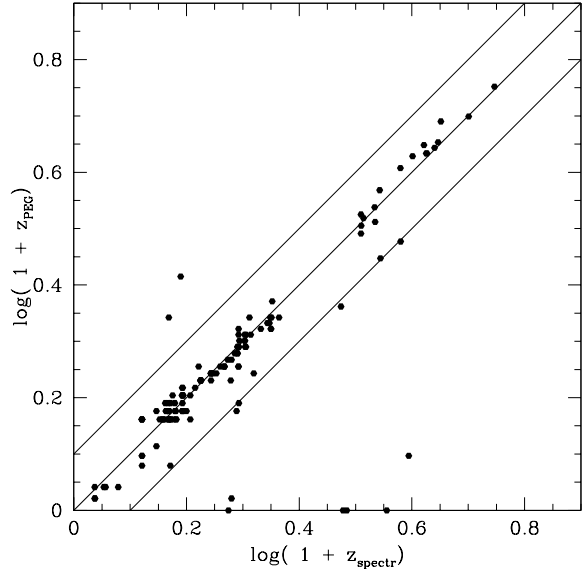


**Figure 23.**  $z_{phot}$  versus  $z_{spectr}$ , from Le Borgne and Rocca (2002).

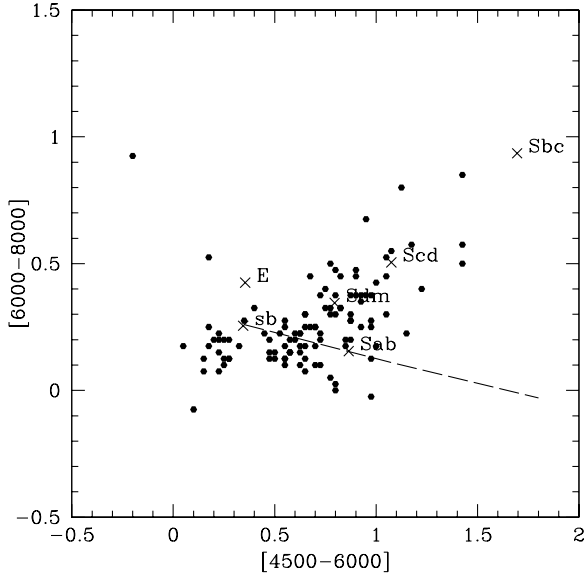


**Figure 22.**  $[6000]-[8000]$  versus  $[4500]-[6000]$  for HDF-N galaxies with  $z = 3.0 \pm 0.4$ . Loci for template galaxies at  $z = 3$ , together with reddening line for starburst template (extending to  $E(B-V) = 1.0$ ) are shown.

range of photometric bands and a narrow range of redshift. Fig 23 shows the excellent results reported by Le Borgne and Rocca-Volmerange (2002) for HDF-N galaxies with photometric data in 7 bands. However the inclusion of additional parameters in the modelling to characterize the star-formation history in-

evitably results in increased aliasing as can be seen in Fig 23 and Table 2.

It is also of interest to ask whether galaxies do really represent a small set of star-formation histories, as assumed by Le Borgne and Rocca-Volmerange (2002). Their main parameter characterizing sed is  $\nu$ , where  $SFR = \nu M_{gas}$  (they also have assumptions about infall and galactic winds). Clearly  $\nu$  determines the ratio  $b = M_*/\dot{M}_* t_0$  which was shown by Larsen and Tinsley (1974) and Scalo (1986) to characterise the Hubble sequence. In practice, as can be seen from Fig 4 of Bruzual and Charlot (1993), galaxy sed consist of two almost independent components; (a) stars formed more than 1 billion years ago, which for a fixed IMF produce an sed peaking in the near infrared which is almost independent of the history of how those stars were formed and only carries (at low resolution at any rate) information on the total mass of stars formed, (b) stars formed less than a billion years ago, which generate an sed dominating the blue and uv part of the spectrum. This part of the sed depends sensitively on the details of the recent star formation rate and whether there have been recent starbursts. It seems possible that the form of the blue-uv part of the spectrum may be uncorrelated with  $b$ , since there is no guarantee that the past billion years of a galaxy's life are typical of its long-term past.

I have therefore investigated deconvolution of galaxy sed into these two components (a) and (b), extending an approach followed by Rowan-Robinson (2001) in modelling galaxy counts. I assume that the elliptical galaxy sed represents component (a) and have then subtracted a multiple of this from the other 5 sed types to fit their red-ir spectrum. The 5 blue-

uv residues are taken to be representative of typical recent star formation histories. Each galaxy sed is then fitted with an arbitrary combination of components (a) and (b), with the normalisation constants essentially specifying  $M_*$  and  $\dot{M}_*$ , respectively. However it is convenient to characterise the ratio of old to young stars by a parameter  $f_{old}$  such that this is 1 when the sed exactly reproduces the original sed template. I have applied this method only to the HDF-N 7-band data because we need near infrared data to get a good determination of  $M_*$ . This method should be very powerful when applied to SIRTf-IRAC data, especially where multiband optical data is also available.

A small number of additional aliases (see Table 2) are generated by the inclusion of this new parameter  $f_{old}$ , which I allow to range logarithmically between 0.04 and 25.

Figure 24 shows a plot of  $M_*/\dot{M}_*t_0$  versus redshift, with the curves corresponding to different star-formation scenarios, varying the value of the exponential parameter  $Q$  used by Rowan-Robinson (2001) - see Appendix. The broad trend is as expected, with higher values of  $b$  towards the past. This is a more powerful demonstration of the evolution of galaxy sed than merely showing that consistent redshifts are obtained if an evolutionary scenario is used. A wide range of value of  $Q$  is needed to understand the distribution of  $b$  with  $z$ . Star-formation was assumed to be initiated at  $z_i = 10$  for this family of curves. To understand galaxies with very low values of  $b$  (very weak bulge components) at  $z = 0.5-2$  it is necessary to assume that some galaxies started to form stars only at much later redshift.

Figure 25 shows a plot of  $M_*/\dot{M}_*t_0$  versus uv sed type, showing a general trend but poor correlation in detail. If there were a true Hubble sequence characterised only by  $\nu$  or  $Q$ , then the points would have fallen on a single locus. In fact there is a great deal of scatter and a wide range of uv sed types can correspond to a single value of  $b$ . Thus there is not a very strong correlation between the recent star-formation history of a galaxy and its integrated history (which determines its Hubble type and bulge-to-disc ratio).

### 3 STAR FORMATION HISTORY

I now pull together estimates of the star-formation history derived from the photometric redshift methods described above, corrected for the effects of dust extinction, together with other infrared and submillimetre estimates which should be independent of dust extinction.

#### 3.1 Estimates from HDF

In the case of the HDF data the extinction at 2800 Å is derived using Milky Way grain properties and

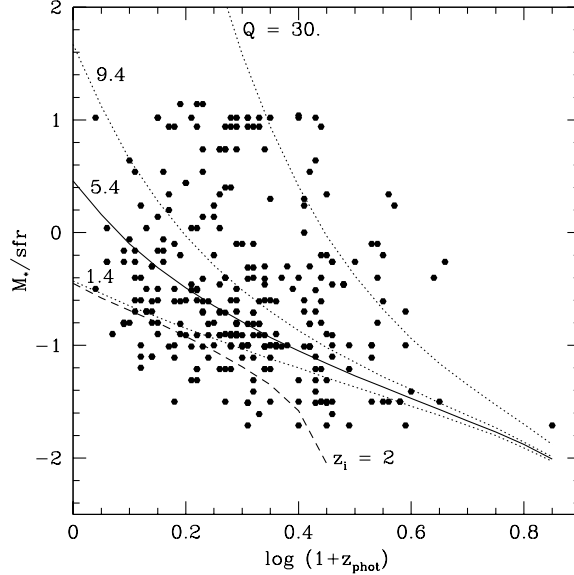


**Figure 24.** Plot of  $M_*/\dot{M}_*t_0$  versus redshift. Curves for simple star-formation histories of the form used by Rowan-Robinson (2001) are shown for  $Q = 1.4, 5.4, 9.4$  and  $30$ , with  $P = 1.2, z_i = 10, \Omega_o = 1$ , in each case. The broken curve corresponds to  $Q = 1.4, z_i = 2$ .

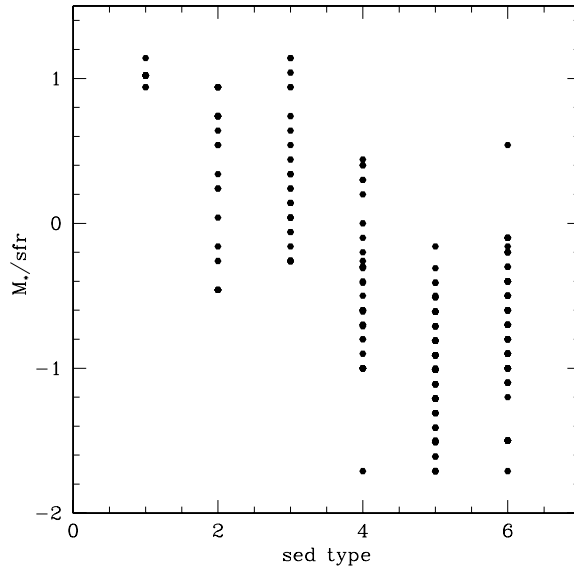


**Figure 25.** Plot of  $M_*/\dot{M}_*t_0$  versus sed type.

using the evolution of  $\langle A_V(z) \rangle$  derived in section 2.2. The net correction,  $10^{0.4A_{2800}}$ , ranges from 2.1 at  $z=0$ , 2.9 at  $z=1$ , to 1.7 at  $z=2$ , 1.3 at  $z=3$  and 1.16 at  $z=4$ . Most estimates of dust correction factors to be applied to high redshift star-forming galaxies range from 2-7 (Meurer et al 1997, 1999, Pettini et al 1998, Steidel et al 1999). Tresse and Maddox (1998) derive

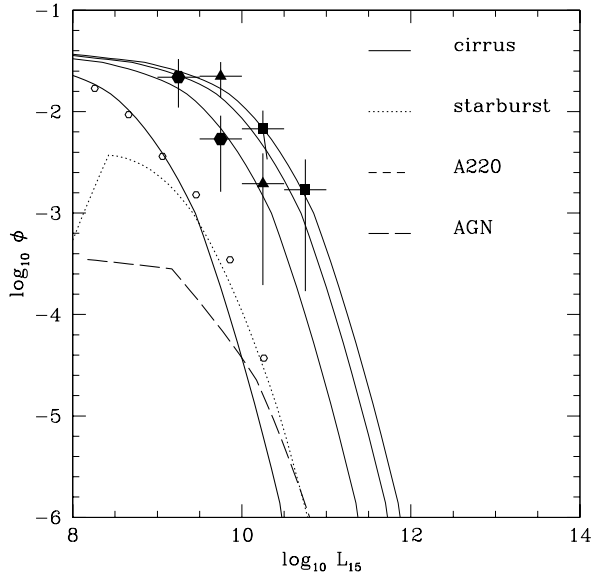


**Figure 26.** Luminosity function at  $15 \mu\text{m}$  for different components from the model of Rowan-Robinson (2001), compared with revised estimate from the ISO survey of the HDF (filled circles:  $z = 0.4\text{-}0.7$ , triangles:  $z = 0.7\text{-}1.0$ , squares:  $z = 1.0\text{-}1.3$ ), and the local estimate of Xu et al (2000, open circles).

a correction factor of 2.5 from a comparison of H $\alpha$  and optical data for  $z = 0.3$  galaxies from the CFRS survey. The corrections I have applied at  $z = 3$  and 4 are much smaller than those assumed by Steidel et al (1999). The latter are based on an assumed  $E(B-V) = 0.15$ , derived from the (G-R) colour distribution, and the assumption of a Calzetti (1997) extinction law. As discussed in the previous section, it is clearly very risky to estimate dust extinction from a single colour. Some doubts on the validity of the Calzetti extinction law have been raised by Rowan-Robinson (2003).

### 3.2 New 15 and 850 $\mu\text{m}$ estimate

Rowan-Robinson et al (1997) gave an estimate for the star formation rate based on ISO detections (mainly  $15 \mu\text{m}$ ) of HDF-N galaxies. Aussel et al (1998) have given a reanalysis of these data using a wavelets method, which confirms the reality of virtually all the detections used by Rowan-Robinson (1997). There is also reasonably good agreement of the  $15 \mu\text{m}$  fluxes used in the two studies. Only source 3 in Table 1 of Rowan-Robinson et al (1997) is not confirmed as a starburst galaxy. Source 2 is not detected by Aussel et al (1998) but is confirmed as a starburst galaxy by Richards et al (1998).

Using the noise contours provided by Aussel et al (1998), I have used a 13.5 sq arcmin area of HDF-N and the Hubble Flanking Fields defined by  $7 \tau_w > 150 \text{ mJy}$  to estimate the  $15 \mu\text{m}$  luminosity function

in different redshift bins using the Aussel et al  $15 \mu\text{m}$  fluxes. There are 22 ISO  $15 \mu\text{m}$  sources within this area, above this flux-limit. Spectroscopic redshifts are available in the Hawaii catalogue for 17 of these, and I have used my photometric redshift estimates (see section 2.1 above) for the remainder. Figure 26 shows the  $15 \mu\text{m}$  luminosity functions for redshift bins 0.4-0.7, 0.7-1.0, and 1.0-1.3. The zero redshift luminosity function of Rowan-Robinson (2001) is also shown together with the locally observed estimates by Xu et al (2000). The luminosity function is also shown shifted by an appropriate pure luminosity evolution for each of the 3 redshift bins. From these shifts I estimate the star-formation rates in these redshift bins. These estimates based on luminosity functions are probably more reliable than estimates made by simply adding all luminosities, as in Rowan-Robinson et al (1997). I have also applied the same method to the  $850 \mu\text{m}$  data HDF-N of Hughes et al (1998), shown in Fig 27. For comparison, Barger et al (2000) derived a star formation rate a factor of 3 higher.

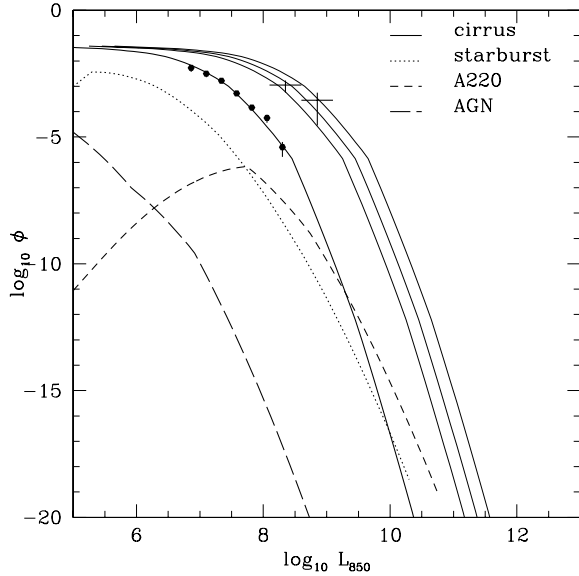
### 3.3 Global star-formation history

Figure 28 shows the star formation history derived either from ultraviolet or H $\alpha$  data with correction for reddening, or from far infrared or submillimetre data under the assumption that most ultraviolet and visible light from star forming regions is absorbed by dust. The curve corresponds to the model used by Rowan-Robinson (2001) to fit multi-wavelength source-counts and the spectrum of the background radiation. At  $z = 0$  it is drawn through the local estimate derived from the uv luminosity-density by Rowan-Robinson (2003).

Haarsma et al (2000) have given estimates of star-formation rates as a function of redshift based on deep VLA surveys of HDF-N and the HFF. These show the same steep rise with redshift as the ISO estimates, but are typically a factor of two higher.

The different estimates used in Fig 28 agree surprisingly well with each other and with the model. The estimates derived from HDF-N and -S lie somewhat below the ISO estimates. The surveys planned with SIRTIF will be able to resolve these discrepancies.

It is relatively straightforward to transform the star-formation as a function of redshift to a different cosmological model. Figure 29 shows the same data as Fig 28 transformed to a model with curvature constant  $k = 0$ ,  $\lambda_o = 0.7$ , together with the best fit star-formation history used in this model by Rowan-Robinson (2001) to fit source-counts and background radiation from optical to submm wavelengths. Both model history and observations have to decline at higher redshifts in this cosmological model because of the greater volume element available per redshift interval.



**Figure 27.** Luminosity function at  $850 \mu\text{m}$ , compared with local data of Dunne et al (2000, filled circles) and with revised estimate from the SCUBA survey of the HDF.

#### 4 CONCLUSIONS

(1) I have investigated the problem of aliasing for photometric redshift estimates and find that it is a serious problem if less than 4 photometric bands are used. Where possible I have compared my photometric redshift estimates with those from other studies.

(2) With reasonable restrictions, it is possible to determine the dust extinction as well as the photometric redshift, provided 5 or more photometric bands are available. The expected evolution of  $\langle A_V(z) \rangle$  with redshift is seen. The extinction is higher than locally at  $z=0.5-1.5$ , and lower at  $z > 2$ .

(3) Deconvolving uv-to-ir sed into an old star and young star component allows determination of  $M_*$  and  $\dot{M}_*$  for each galaxy, as well as  $z_{phot}$  and  $A_V$ , provided there are a reasonable number of photometric bands available. The expected trend of  $b = \dot{M}_*/\langle \dot{M}_* \rangle$  increasing to the past is seen. However there is a great deal of scatter in the relation between  $b$  and uv sed type, showing that the recent star-formation history is not very well correlated with the long-term history of a galaxy.

(4) I have calculated the  $2800 \text{ \AA}$  luminosity function and star-formation rate for a large sample of HDF-N (2490) and HDF-S (28719) galaxies, using photometric redshifts, for the redshift range 0.2-5. The results agree well with those from a variety of other uv estimates. The luminosity functions are consistent with a steep faint-end slope ( $\alpha = 1.6$ ) at all redshifts.

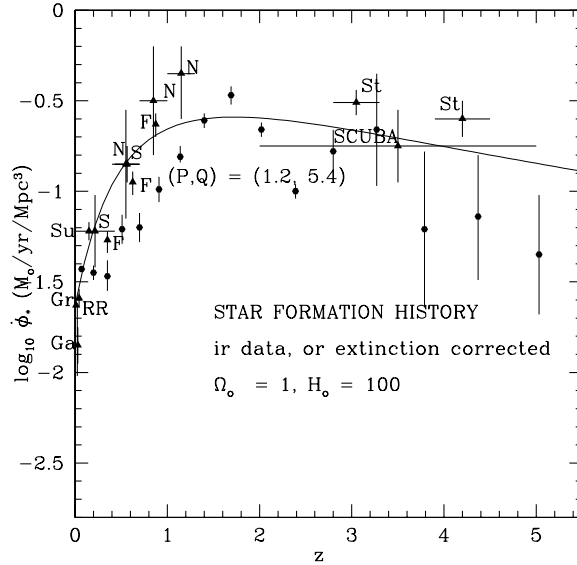


**Figure 28.** Star formation history derived for an  $\Omega_0 = 1$  universe from infrared (N: ISO-HDF-N data (Rowan-Robinson et al 1997) as reanalysed in the present paper, S: ISO-HDF-S data of Mann et al (2001), F: Flores et al 1999 ISO survey of CFRS field), and submillimeter (SCUBA,  $850 \mu\text{m}$ : Hughes et al 1998 data, as reanalysed in the present paper) data, from ultraviolet data with correction for effects of dust, from Gallego et al (1995, Ga), Sullivan et al (2001, Su), both corrected by a factor 2 for dust extinction, Gronwall (1998, Gr), Rowan-Robinson (2003, RR) and Steidel et al (1998, St) (triangles) and from the analysis of photometric redshifts of HDF galaxies given in section 3, corrected for dust extinction at  $2800 \text{ \AA}$  as described in section 2.2. The model shown is chosen to fit the far infrared and submm counts (Rowan-Robinson 2001),  $(P,Q) = (1.2, 5.4)$ , and has been drawn through a local,  $z = 0$ , value for  $\log_{10} \dot{\phi}_* = -1.63$  (taken from the analysis of local galaxies with uv and far ir data by Rowan-Robinson (2003)).

#### 5 ACKNOWLEDGEMENTS

I thank Seb Oliver, Thomas Babbedge, and Maria Polletta for helpful discussions, Daniel Le Borgne for supplying his photometric redshift catalogue, and an anonymous referee for helpful comments.

#### REFERENCES

- Adelberger K.L., Steidel C.C., 2000, ApJ 544, 218  
 Arnouts S., Christiani S., Moscardini L., Matarrese S., Lucchin F., Fontana A., Giallongo E., 1999, MN 310, 540  
 Aussel H., Cesarsky C.J., Elbaz D., Starck J.L., 1999, AA 342, 313  
 Barger A.J., Cowie L.L., Richards .A., 2001, ApJ (in press), astro-ph/0001096  
 Bolzonella M., Miralles J.-M., Pello R., 2000, AA 363, 476  
 Bruzual A.G., and Charlot, S., 1993, ApJ 405, 538

**Table 1.** Proportions of different galaxy sed types in HDF-N as a function of redshift

$z =$	0.1	0.3	0.5	0.7	0.9	1.1	1.3	1.5	1.7	1.9	2.1	2.3	2.5
$N_{gal}, (B \leq 29.0) =$	17	62	90	88	107	111	172	172	174	897	124	161	56
% E	11.8	14.5	4.4	9.1	11.2	3.6	0.6	0.0	0.6	0.0	0.0	0.6	5.4
% Sab	0	3.2	3.3	0	2.8	5.4	2.9	6.4	1.7	11.5	18.5	4.3	1.8
% Sbc	11.8	3.2	4.4	1.1	6.5	1.8	0.6	1.2	3.4	3.4	4.0	1.2	1.8
% Scd	41.2	21.0	17.8	18.2	7.5	21.6	5.2	6.4	8.0	6.9	4.8	6.8	8.9
% Sdm	11.8	17.8	31.1	46.6	19.6	37.8	19.2	6.4	13.8	42.5	46.0	6.2	5.4
% starburst	23.5	37.1	38.9	25.0	52.3	29.7	71.5	79.7	72.4	35.6	26.6	80.7	76.8

**Table 2.** Objects in HDF-N for which at least one photometric redshift method has a problem. Columns give name, Fernandez-Soto (FLY) et al (1999) number, spectroscopic redshift, and photometric redshifts given by FLY(1999), FLY(2001), le Borgne and Rocca-Volmerange (2002), present work template method (RR,T), template method + arbitrary  $A_V$  (RR,TAV), two component method (RR,C), two component method + arbitrary  $A_V$ . Bottom line gives total number of problem sources for each method, defined as  $\Delta = |\log_{10}((1 + z_{ph})/(1 + z_{sp}))| > 0.10$ .

name	FLY no.	$lg_{10}$ ( $1 + z_{sp}$ )	$lg_{10}$ ( $1 + z_{FLY}$ )	$lg_{10}$ ( $1 + z_{FLY01}$ )	$lg_{10}$ ( $1 + z_{BR}$ )	$lg_{10}$ ( $1 + z_{RR,T}$ )	$lg_{10}$ ( $1 + z_{RR,TAV}$ )	$lg_{10}$ ( $1 + z_{RR,C}$ )	$lg_{10}$ ( $1 + z_{RR,CAV}$ )
3-875.0	48	0.484	0.483	0.519	0.00	0.47	0.47	0.47	0.46
4-332.1	315	0.225	0.326	0.238	0.00	0.28	0.25	0.26	0.25
3-550.1	334	0.577	0.435	0.000	0.00	0.48	0.53	0.48	0.54
4-289.0	444	0.599	0.483	0.567	0.000	0.55	0.53	0.55	0.56
4-928.1	466	0.304	0.283	0.286	0.290	0.29	0.20	0.27	0.15
4-445.0	517	0.544	0.365	0.540	0.447	0.48	0.44	0.42	0.43
3-243.0	568	0.627	0.615	0.653	0.630	0.63	0.63	0.63	0.47
4-254.0	653	0.279	0.204	0.201	0.230	0.18	0.13	0.21	0.23
4-52.111	687	0.595	0.107	0.100	0.097	0.63	0.63	0.63	0.46
4-639.1	702	0.555	0.000	0.531	0.000	0.57	0.57	0.58	0.58
4-946.0	716	0.289	0.225	0.230	0.176	0.26	0.19	0.21	0.21
2-585.1111	1016	0.474	0.422	0.422	0.362	0.49	0.44	0.44	0.43
2-251.0	1018	0.293	0.265	0.267	0.190	0.27	0.20	0.21	0.19
2-449.1	1044	0.478	0.017	0.543	0.000	0.49	0.49	0.49	0.49
2-82.1	1062	0.514	0.435	0.004	0.512	0.53	0.54	0.54	0.56
number	with	$\Delta > 0.10$	7	3	10	0	3	1	5

Le Borge D. and Rocca-Volmerange B., 2002, AA 386, 446  
 Buat V., Donas J., Deharveng J.-M., 1987, AA 185, 33  
 Budavari T., Szalay A.S., Connolly A.J., Csadaï I., Dickinson M., 2000, AJ 120, 1588  
 Calzetti D., 1997, AJ 113, 162  
 Calzetti D., and Kinney A.L., 1992, ApJ 399, L39  
 Calzetti D., Heckman T.M., 1999, ApJ 519, 27  
 Cohen J.G., Hogg D.W., Blandford R., Cowie L.L., Hu E., Songaila A., Shobbell P., Richberg K., 2000, ApJ 538, 29  
 Cohen J.G., 2001, AJ 121, 2895  
 Connolly A.Z., Szalay A.S., Dickinson M., Subbarao M.U., Brunner P.J., 1997, ApJ 486, L11  
 Cram L., 1998, ApJ 507,155

Erb D.K., Shapley A.E., Steidel C.C., Pettini M., Adelberger K.L., Hunt M.P., Moorwood A.F.M., Cuby J.-G., 2003, ApJ (in press), astro-ph/0303392  
 Fernandez-Soto A., Lanzetta K.M., Yahil A., 1999, ApJ 513, 34 (FLY)  
 Fernandez-Soto A., Lanzetta K.M., Chen H.-W., Pascaelle S., Yahata N., 2001, ApJS 135, 41  
 Flores H. et al, 1999, ApJ 517, 148  
 Fontana A., D'Odorico S., Poli F., Giallongo E., Arnouts S., Christiani S., Moorwood A., Saracco P., 2000, MN 339, 260  
 Gallego J., Zamorano J., Aragon-Salamanca A., Rego M., 1995, ApJ 455, L1  
 Glazebrook K., Blake C., Economou F., Lilly S., Colless

**Table 3.** Galaxies in HDF-N with  $z_{phot} > 5$ .

name	I	$z_{phot}$	$z_{sp}$	$z_{FLY}$	$n_{type}$	$n_{band}$
3-951.1	25.83	6.08	5.339	5.72	4	3
4-625.1	25.19	5.17	4.585	4.52	4	4
4-314.0	27.38	6.08	0.000	4.76	3	2
4-473.0	27.95	6.08	5.607	5.64	1	2
4-842.0	28.02	6.08	0.000	4.64	1	2
4-148.0	28.78	5.46	0.000	1.24	4	2
4-169.0	26.61	6.08	0.000	5.64	3	3
3-516.0	27.22	5.92	0.000	4.76	1	2
3-489.0	27.06	6.08	0.000	4.76	3	2
3-457.0	27.33	6.08	0.000	5.48	3	2
3-387.0	26.28	5.31	0.000	0.84	2	4
3-324.0	28.61	5.46	0.000	5.20	3	2
3-255.0	27.50	5.92	0.000	4.92	4	2
3-242.0	27.72	5.31	0.000	0.68	3	2
3-228.0	27.25	5.76	0.000	5.04	1	2
3-153.0	27.20	6.08	0.000	5.32	4	2
4-799.0	27.67	6.08	0.000	4.84	1	2
4-884.0	28.37	5.46	0.000	4.40	5	2
4-310.0	28.42	6.08	0.000	4.84	1	2
3-44.0	27.72	5.76	0.000	4.80	1	2
2-282.0	26.14	5.76	0.000	4.36	2	3
2-892.0	26.50	5.76	0.000	4.72	4	2
2-156.0	27.62	5.46	0.000	0.72	4	2
2-925.0	28.26	5.31	0.000	4.60	3	2
2-364.0	28.22	6.08	0.000	4.80	1	2
2-490.0	28.60	5.03	0.000	0.00	4	2
2-882.0	27.35	5.31	0.000	0.00	4	2
3-839.0	24.66	5.92	0.000	0.00	5	3
3-874.0	27.97	5.76	0.000	0.00	3	2
3-951.0	25.58	5.76	0.000	0.00	5	2
3-965.1112	25.53	5.31	0.000	0.00	4	3
4-625.2	27.49	5.61	0.000	0.00	1	2
4-683.0	29.72	5.03	0.000	0.00	1	2

- M., 1999, MN 306, 843
- Gronwall C., 1998, in 'Dwarf Galaxies and Cosmology', eds T.X.Thuan, C.balkowski, V.Cayatte, J.Tran Thanh Van, (Editions Frontieres), astro-ph/9806240
- Gwynn S.D.J. and Hartwick F.D.A., 1996, ApJ 468, L77
- Haarsma D.B., Partridge R.B., Windhorst R.A., Richards E.A., 2000, ApJ 544, 641
- Hogg D.W., et al, 1998, AJ 115, 1418
- Hopkins et al, 2001, AJ 122, 288
- Hughes D.H., Serjeant S., Dunlop J., Rowan-Robinson M., Blain A., Mann R.G., Ivison R., Peacock J., Efstathiou A., Gear W., Oliver S., Lawrence A., Longair M., Goldschmidt P., Jenness T., 1998, Nat 394, 241
- King A.J., Rowan-Robinson M., 2003, MN 339, 260
- Lanzetta K.M., Yahil A., Fernandez-Soto A., 1996, Nature 381, 759
- Lanzetta K.M., Yahata N., Pascarelle S., Chen H.-W., Fernandez-Soto A., 2002, ApJ 570, 492
- Lilly, S.J., Le Fevre, O., Hammer, F., Crampton, D., 1996, ApJ 460, L1
- Madau, P., Ferguson, H.C., Dickinson, M.E., Giavalisco, M., Steidel, C.C., Fruchter, A., 1996, MNRAS 283, 1388
- Madau, P., 1998, in 'The Hubble Deep Field', ed. M.Livio, S.M.Fall and P.Madau (STScI Symposium Series) astro-ph/9709147
- Madau P., Pozzetti L., Dickinson M., 1998, ApJ 498, 106
- Mann R.G. et al, 2001, MN (submitted)
- Mazzarella J.M., Balzano V.A., 1986, ApJS 62, 751
- Meurer G.R., Heckman T.M., Leitherer C., Kinney A., Robert C., Garnett D.R., 1995, AJ 110, 2665
- Meurer G.R., Heckman T.M., Lehnert M.D., Leitherer C., Lowenthal J., 1997, AJ 114, 54
- Meurer G.R., Heckman T.M., Calzetti D., 1999, ApJ 521, 64
- Mobasher, B., Rowan-Robinson, M., Georgakakis, A., Eaton, N., 1996, MN 282, L7
- Mobasher M. and Mazzei P., 1999, in 'Photometric Redshifts and High Redshift Galaxies', Weymann et al. Eds., Astr.Soc. of Pac.Conf. Series 191, astro-ph/9907210
- Pascarelle S.M., Lanzetta K.M., Fernandez-Soto A., 1998, ApJ 508, L1
- Peacock J.A., Rowan-Robinson M., Blain A.W., Dunlop J.S., Efstathiou A., Hughes D.H., Jenness T., Ivison R.J., Lawrence A., Longair M.S., Mann R.G., Oliver S.J., Serjeant S., 2000, MN 318, 535
- Pei Y.C., Fall M.S., Hauser M.G., 1999, ApJ 522, 604
- Pettini M., Kellogg M., Steidel C.C., Dickinson M., Adelberger K.L., Giavalisco M., 1998, ApJ 508, 539
- Pozzetti L., Madau P., Ferguson H.C., Zamorani G., Bruzual G.A., 1998, MN 298, 1133

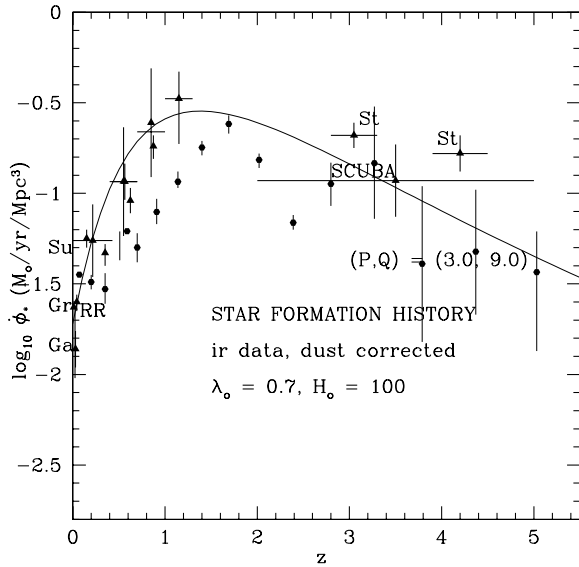


**Figure 29.** Star formation history derived from infrared data, from ultraviolet data with correction for effects of dust, and from the analysis of photometric redshifts of HDF galaxies given in section 3 for an  $\Omega_o = 0.3$ ,  $\lambda_o = 0.7$ ,  $H_o$  cosmology. The model shown is chosen to fit the far infrared and submm counts (Rowan-Robinson 2001), (P,Q) = (3.0, 9.0), and have been drawn through a local,  $z = 0$ , value for  $\log_{10}\dot{\phi}_* = -1.63$  (Rowan-Robinson 2003).

- Richards E.A. et al, 1998, AJ 116, 1039  
 Riess A.G. et al, 2001, ApJ (submitted), astro-ph/0104455  
 Rodighero G., Franceschini A., Fasano G., 2001, MN 324, 491  
 Rowan-Robinson M. et al, 1997, MN 289, 490  
 Rowan-Robinson M., 2001, ApJ 549, 745  
 Rowan-Robinson M., 2003, MNRAS (in press)  
 Saunders, W., Rowan-Robinson, M., Lawrence, A., Efstathiou, G., Kaiser, N., Frenk, C.S., 1990, MN 242, 318  
 Shapley A.E., Steidel C.C., Adelberger K.L., Dickinson M., Giavalisco M., Pettini M., 2001, ApJ 562, 95  
 Steidel C.C., Adelberger K.L., Dickinson M., Giavalisco M., Pettini M., Kellogg M., 1998, ApJ 492, 428  
 Steidel C.C., Adelberger K.L., Giavalisco M., Dickinson M., Pettini M., 1999, ApJ 519, 1  
 SubbaRao M.U., Connolly A.J., Szalay A.S., 1996, AJ 112, 129  
 Sullivan M., Treyer M.A., Ellis R.S., Bridged T.J., Milliard B., Donas J., 2000, MN 312, 442  
 Sullivan M., Mobasher B., Chan B., Cram L., Ellis R., Treyer M., Hopkins A., 2001, ApJ 558, 72  
 Teplitz H.I., Hill R.S., Malumuth E.M., Collins N.R., Gardner J.P., Palunas P., Woodgate B.E., 2001, ApJ 548, 127  
 Thompson R.I., Weymann R.J., Storrie-Lombardi L.J., 2001, ApJ 546, 694  
 Tresse L., Maddox S.J., 1998, ApJ 495, 691  
 Treyer M.A., Ellis R.S., Milliard B., Donas J., Bridges T.J., 1998, MN 300, 303  
 Vijh U.P., Witt A.N., Gordon K.D., 2003, astro-

ph/0301121

- Williams R.E. et al, 1996, AJ 112, 1335  
 Wilner D.O., Wright M.C.W., 1997, ApJ 488, L67  
 Xu C., 2000, ApJ 541, 134  
 Yoshii Y. and Takahara F., 1988, ApJ 326, 1

## 6 APPENDIX: STAR FORMATION HISTORY MODEL

For a simple closed box galaxy model with constant yield and instantaneous recycling, in which all the heavy elements in the interstellar medium are assumed to be in the form of dust, the mass of gas  $M_{gas}(t)$ , stars  $M_*(t)$ , heavy elements  $M_Z$ , and dust  $M_{dust}(t)$ , satisfy

$$dM_*/dt = \dot{\phi}_* = -dM_{gas}/dt, \quad (A.1)$$

$$M_Z = M_{dust} = kM_*, \quad (A.2)$$

$$\dot{M}_{dust} = (k - Z)\dot{\phi}_*, \quad (A.3)$$

$$M_{dust} = ZM_{gas}, \quad (A.4)$$

where  $k$  is the yield,  $Z$  is the metallicity of the ism, and  $\dot{\phi}_*$  is the star-formation rate.

Substituting (A.4) in (A.3) and using (A.1), it follows that

$$M_{gas}\dot{Z} = -k\dot{M}_{gas}$$

and hence (Pei et al 1999) that

$$Z = k \ln(M_{gas}(0)/M_{gas}(t)) \quad (A.5)$$

and

$$M_{dust}(t) = kM_{gas}(t) \ln(M_{gas}(0)/M_{gas}(t)). \quad (A.6)$$

Rowan-Robinson (2001) has shown that star-formation histories of the form

$$\dot{\phi}_* = \alpha t^m e^{-\nu t} \quad (A.7)$$

provide an extremely effective fit to source-counts and redshift distributions from optical to submillimetre wavelengths, with the assumption that characteristic luminosities in galaxies trace  $\dot{\phi}_*(t)$ . In such a model

$$M_*(t) = \alpha_0 M_{gas}(0) \gamma(m+1, \nu t) \quad (A.8) \\ = M_{gas}(0) - M_{gas}(t)$$

where the incomplete gamma function

$$\gamma(m+1, y) = \int_0^y x^m e^{-x} dx, \text{ and}$$

$$\alpha = \alpha_0 \nu^{m+1} M_{gas}(0). \quad (A.9)$$

There is then a critical value of  $\alpha_0$ ,  $\alpha_{0,c} = 1/\Gamma(m+1)$ , such that the gas runs out in the galaxy if  $\alpha_0 > \alpha_{0,c}$ . This, together with the fact that the star-formation rate starts off as zero at  $t = 0$ , rather than at its maximum value, makes models of type (A.7) more versatile and realistic than the usually assumed exponentially declining star-formation rate (Bruzual and Charlot 1993, Pei et al 1999, Fioc and Rocca-Volmerange 2000). Equations (A.6) and (A.8) have

been used to provide the model curves in Figs 20 and 24 of this paper, with the assumption that the visual extinction

$$A_V(t) = (3Q_V/4a\rho_{gr})M_{dust}(t)/\pi R_{gal}^2, \quad (\text{A.10})$$

where  $R_{gal}$ ,  $a$ ,  $\rho_{gr}$ ,  $Q_V$  are characteristic values for the galaxy radius, grain radius, density of grain material, and V-band extinction efficiency. In practice, having specified  $m$ ,  $\nu$  ( $= P, Q/t_0$  in the notation of Rowan-Robinson 2001),  $\alpha_0$  and the parameters in eqn (A.10) are chosen to give a gas fraction of 10% and an  $A_V$  of 0.3 (Rowan-Robinson 2003) at the present epoch.

To fully match the properties of present day galaxies it is necessary to modify eqn (A.1) to take account of both infall of pristine intergalactic gas into galaxies, and outflow of enriched material in supernova-driven winds. Some aspects of inflow can be modelled by extending (A.7) to include density evolution, to match the effects of galaxy merging (Rowan-Robinson 2001). King and Rowan-Robinson (2003) have used such models to improve the fit to optical and near infrared galaxy counts, and shown that the best-fitting models of this type give evolving luminosity functions very similar to those found in hierarchical simulations.

If we take the space-density of galaxies, as in King and Rowan-Robinson (2003) to be modified by a factor  $\rho(z) = (1+z)^n$ , we then need to think of each galaxy at  $z = 0$  broken up into  $\rho(z)$  pieces at  $z$ , so  $R_{gal}(z) = R_{gal}(0)\rho(z)^{-1/3}$  and then

$$A_V(t) = (3Q_V/4a\rho_{gr})M_{dust}(t)\rho(z)^{-1/3}/\pi R_{gal}^2. \quad (\text{A.11})$$

The King and Rowan-Robinson (2003) model for  $\Omega_0 = 1$  has been included in Fig 20, with (A.7) modified to replace  $m$  by  $P - 2n/3$ .